Electronic Supplementary Material (ESI) for Dalton Transactions.

Supplementary Information

Unveiling the Effect of Crystalline Phases of Iron Oxyhydroxide for Highly Sensitive and Selective Detection of Dopamine

Sreejesh Moolayadukkam,[†a] Savithri Vishwanathan,[†a] Byeongsun Jun,[b] Sang Uck Lee[b,c] and H. S. S. Ramakrishna Matte[a]*

a. *Energy Materials Laboratory, Centre for Nano and Soft Matter Sciences, Bangalore, India- 562162.*
b. *Department of Bionano Technology, Hanyang University, Ansan, 15588, Republic of Korea*
c. *Department of Applied Chemistry, Hanyang University, Ansan, 15588, Republic of Korea*

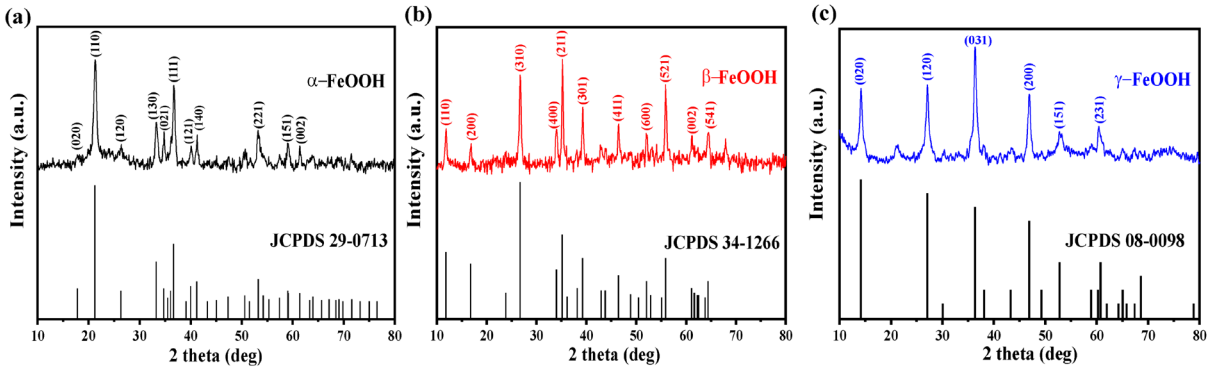

Figure S1. XRD patterns of (a) α-FeOOH, (b) β-FeOOH and (c) γ-FeOOH indexed to corresponding JCPDS references.

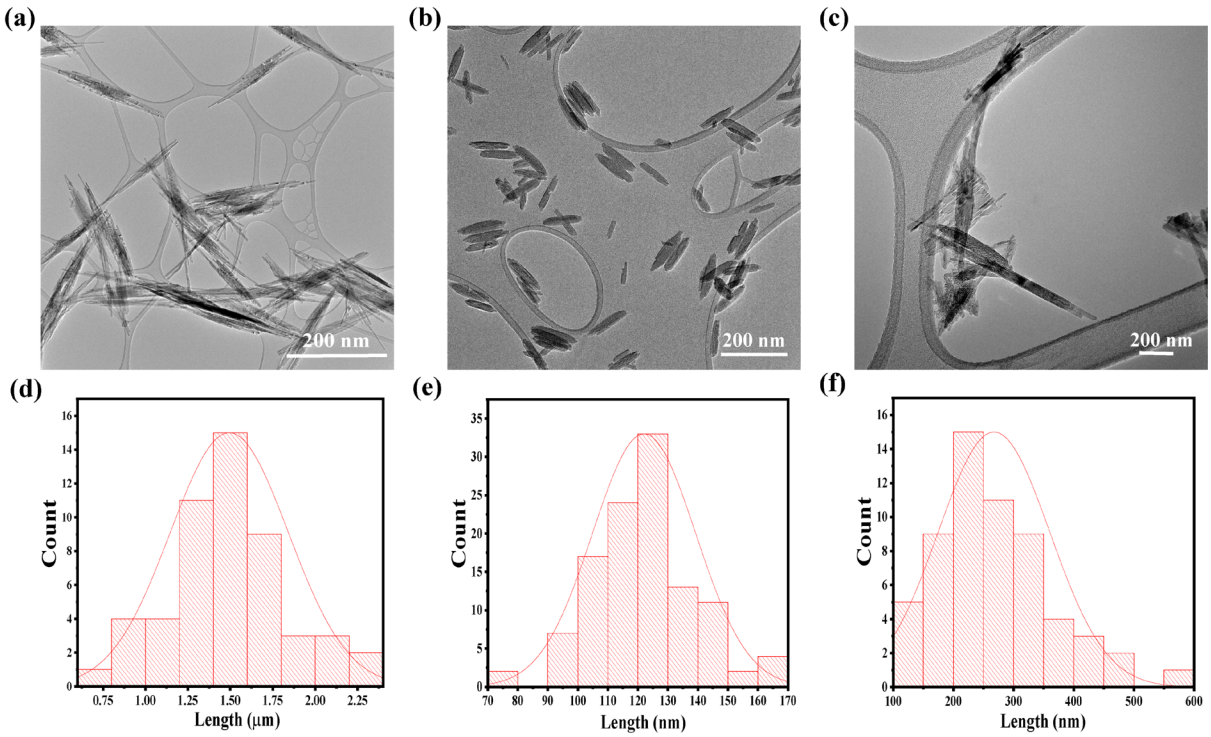

Figure S2. TEM images and size distribution of α-FeOOH (a,d), β-FeOOH (b,e) and γ-FeOOH (c,f)

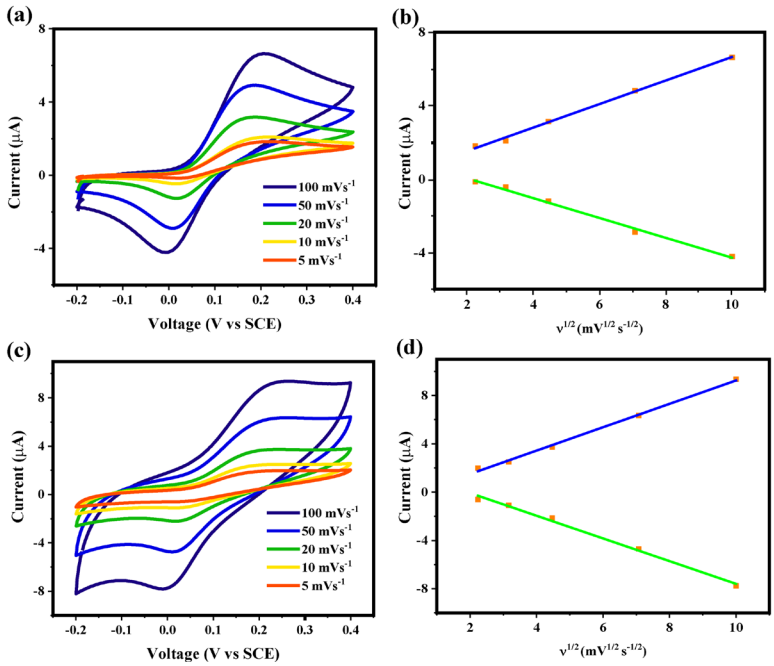

Figure S3. (a), (c) CV at different scan rates; (b), (d) linear plot of peak current vs square root of scan rate for α- and γ-FeOOH respectively.

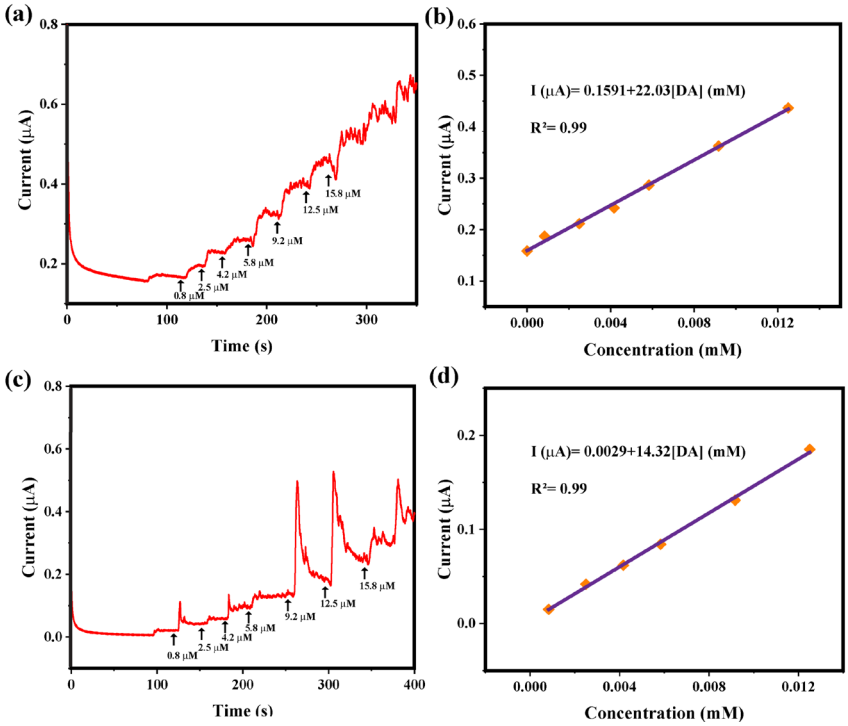

Figure S4. (a), (c) chronoamperometric response with successive addition of DA; (b), (d) calibration curve for linear response of current vs DA concentration for α- and γ-FeOOH respectively.

Table S1. Sensitivity from CA (calibration curve data points in bold):

Concentration (mM)	**Current (µA) (α-FeOOH)**	**Current (µA) (β-FeOOH)**	**Current (µA) (γ-FeOOH)**
0.00083	**0.15829**	**0.02875**	**0.01503**
0.0025	**0.1871**	**0.06607**	**0.04178**
0.00417	**0.21152**	**0.10403**	**0.06189**
0.00583	**0.24219**	**0.13956**	**0.08417**
0.00917	**0.28662**	**0.20493**	**0.13101**
0.0125	**0.36255**	**0.26996**	**0.18503**
0.01583	**0.43671**	**0.33118**	**0.2525**
0.01917	0.48645	0.39703	0.2966
0.0225	0.54627	0.44586	0.36734
0.02583	0.61706	0.50293	0.40222
0.02917		0.55206	0.45593
0.0325		0.59235	0.51178
0.03583		0.64697	
0.03917		0.67688	
0.0425		0.7196	

Calculation of limit of detection (LOD)

The limit of detection (LOD) for the electrocatalysts were determined by chronoamperometry. The measurement was performed without adding the analyte by applying the oxidation potential for a fixed interval of time. The above measurements were repeated five times for each electrocatalyst. At a particular time, the standard deviation (SD) of the current was calculated. The LOD was found using the formula (3×SD)/s where, s is the slope of the calibration curve for obtained from the sensitivity measurements.

Table S2. Comparison with other reported dopamine sensors

Materials	**Sensitivity ($\mu A\ mM^{-1}\ cm^{-2}$)**	**Detection limit (μM)**	**Linear range**	**Ref.**
PPy/graphene	363	2.3	0.1-1 mM	[1]
GO-MWCNT/MnO_2/ AuNP	233.4	0.17	0.5 μM-2 mM	[2]
$Ni(OH)_2$/NiCo-LDHs	83.48	0.017	1.08 mM	[3]
ZnO/CuO	90.9	-	0.001-8 μM	[4]
PEDOT-LSG	0.22 $\mu A\ \mu M^{-1}$	0.33	1-150 μM	[5]
NiAl-LDH/graphene	0.022 $\mu A\ \mu M^{-1}$	9.6	80-400 μM	[6]
Pyrolitic carbon	0.2 $\mu A\ \mu M^{-1}\ cm^{-2}$	2.3	18-270 μM	[7]
AuNPs-rGOS-ITO	62.7	0.06	0.02-40 μM	[8]
PEDOT: PSS/ITO	196	1	0.01-0.9 mM	[9]
α-FeOOH	270.17	0.75	0.83 -12.5 μM	this work
β-FeOOH	**337.51**	**0.56**	**0.83 -12.5 μM**	**this work**
γ- FeOOH	202.83	1.32	0.83 -12.5 μM	this work

Electrochemical surface area (ECSA) determination

1. The double-layer capacitance method

The double-layer capacitance (C_{dl}) was determined in 0.1 M PBS along with analyte solution. Cyclic voltammetry was performed in non-faradic region/double-layer region in potential range from -0.2 V to 0 V *vs.* SCE at various scan rates (5 to 100 mV s^{-1}). The slope of the plot between averaged current: $(I_a+I_c)/2$ ('a' and 'c' denote anodic and cathodic current respectively) at -0.1 V *vs.* SCE versus the scan rate gives C_{dl} (in µF). C_{dl} was then divided by the specific capacitance of the flat standard surface (20-60 µF cm^{-2}) which is considered to be 40 µF cm^{-2} in this study.[10] This gives the electrochemical surface area (ECSA).

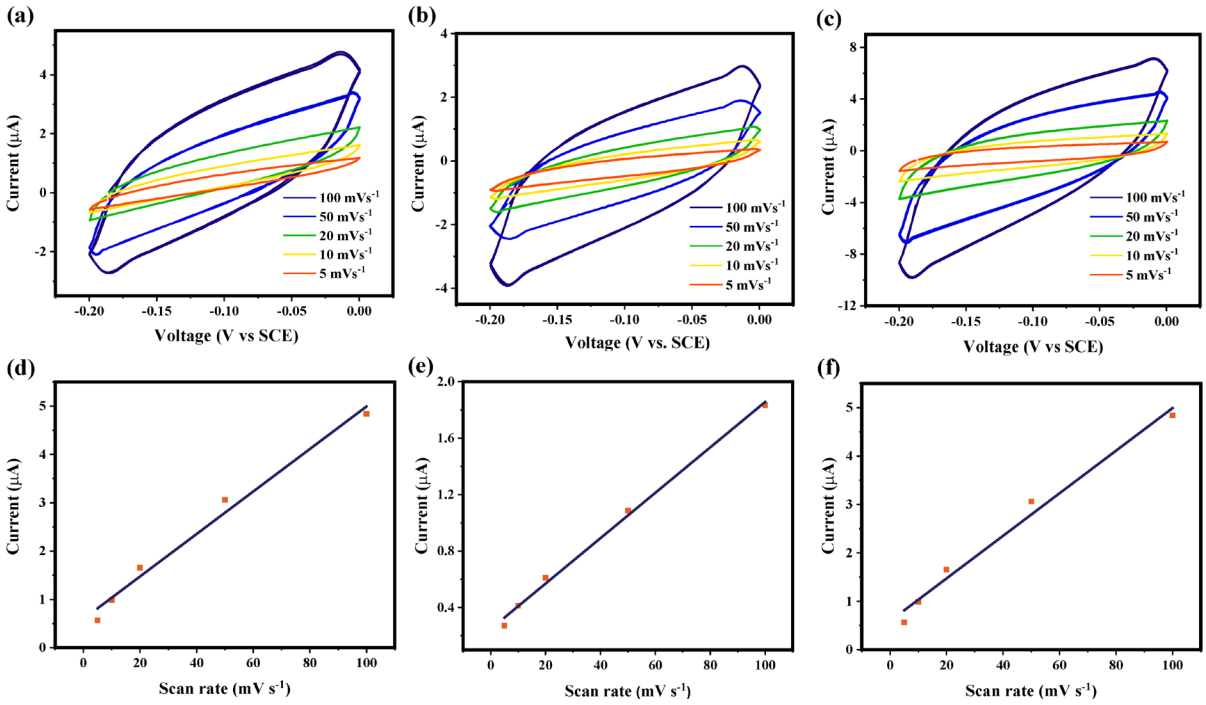

Figure S5. CV of (a) α-FeOOH (b) β-FeOOH and (c) γ-FeOOH at the non-faradaic potential region and (d, e, f) the corresponding average current versus scan rate plots.

2. Randles-Sevcik equation

The Randles–Sevcik equation, which gives the relation between the peak current and square root of the scan rate for a diffusion-controlled electron transfer process, can be used to determine the surface area that is accessible for electron transfer to analyte:

$$I_p = 2.687 \times 10^5 A C n^{3/2} (D\upsilon)^{1/2}$$

where I_p is the peak current (A), A is the electrochemically active surface area (cm^2), C is the concentration of the analyte (mol cm^{-3}), n is the number of electrons involved in the process, D is the diffusion coefficient ($cm^2\ s^{-1}$) (obtained from bibliographic data[11]) and υ is the scan rate ($V\ s^{-1}$).

BET surface area determination

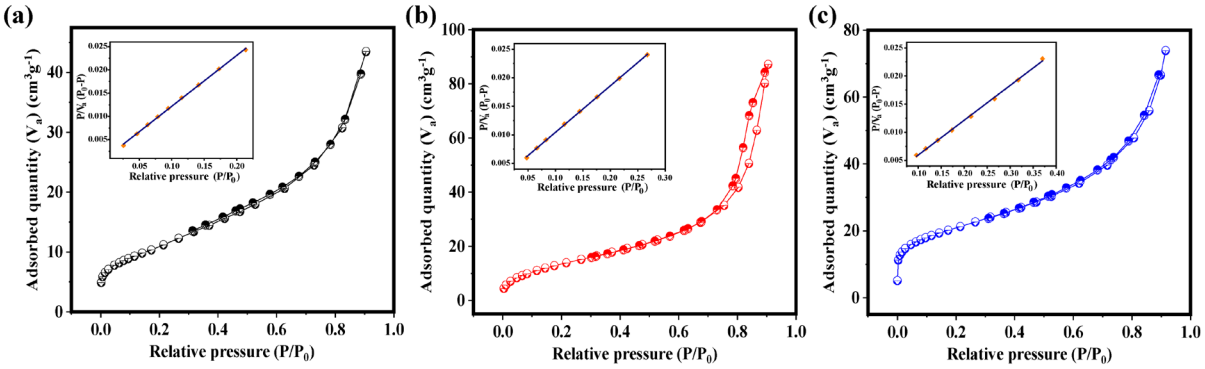

Figure S6. Adsorption isotherms at 77 K and surface area plots (inset) for (a) α-FeOOH (b) β-FeOOH and (c) γ-FeOOH

Determination of active sites

1. Electroactive sites

$$\%\ \text{Electroactive sites} = \frac{\text{ECSA}\ (Randles - Sevcik)}{\text{ECSA}\ (double - layer)} * 100$$

2. Active sites normalized with respect to BET surface area

% Active sites/$m^2\ g^{-1}$ = % Electroactive sites/BET surface area

Table S3. Active site percentage calculation from ECSA and BET surface area.

Electrocatalyst	**ECSA (Randles-Sevcik) (cm^2)**	**ECSA (double-layer) (cm^2)**	**% Electroactive sites**	**BET surface area (m^2 g^{-1})**	**% Active sites/ m^2 g^{-1}**
α-FeOOH	0.0639	0.4635	13.7	39.405	0.35
β-FeOOH	0.0873	0.4022	21.7	51.964	0.42
γ-FeOOH	0.0966	1.0992	9.3	73.361	0.13

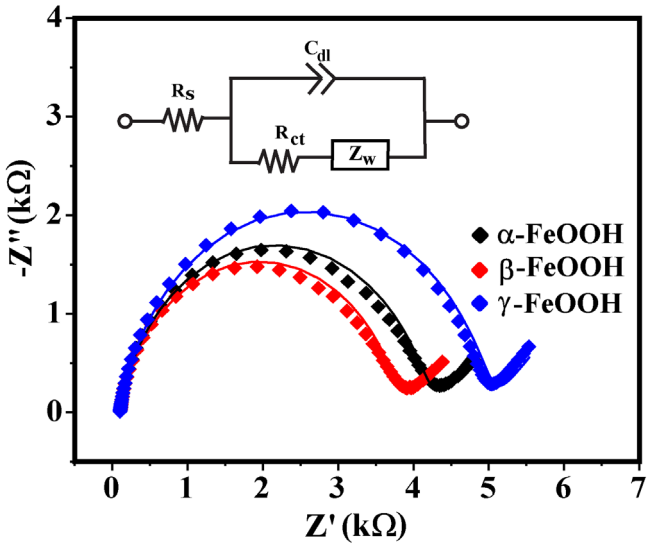

Figure S7. Nyquist plots of FeOOH electrocatalysts in the presence of 10 mM $K_3Fe(CN)_6$ in 0.1 M PBS (pH 7.4).

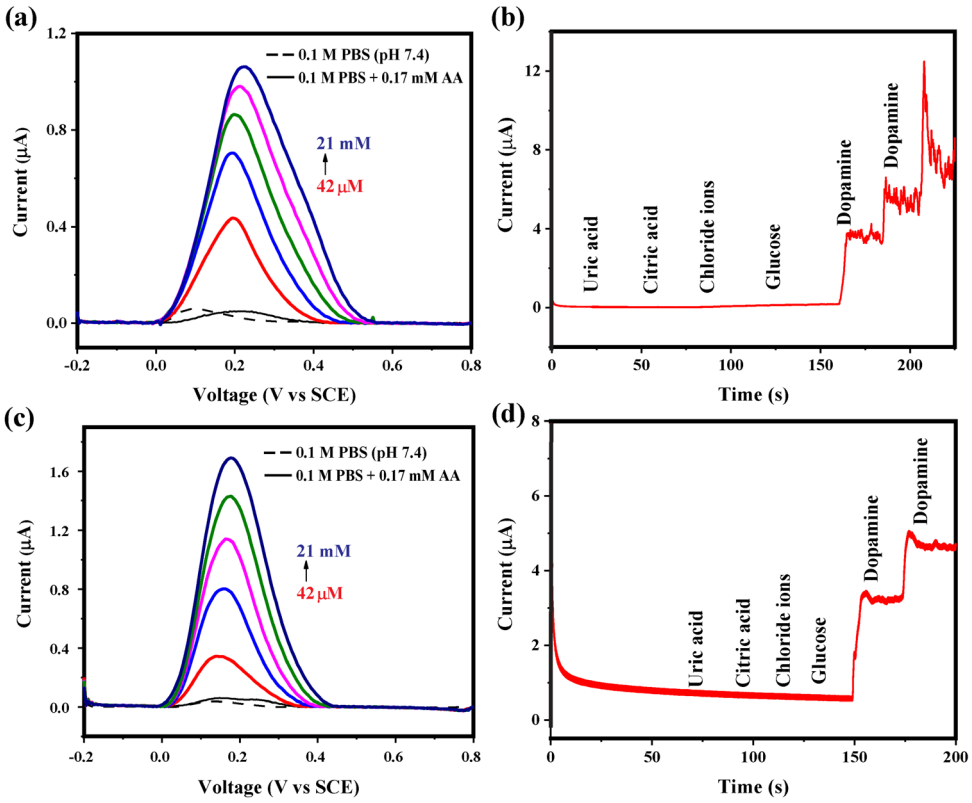

Figure S8. (a, c) DPV measurements with increasing DA concentration in the presence of 0.17 mM AA and (b, d) CA with other interferents for α- and γ-FeOOH respectively

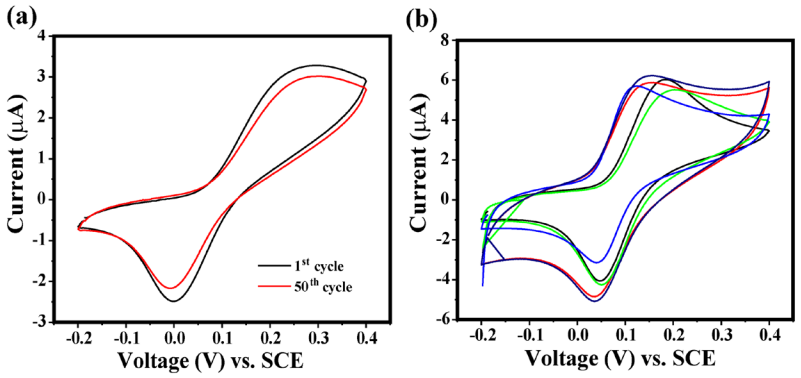

Figure S9. (a) Fifty consecutive voltammograms of β-FeOOH and (b) CV of five different β-FeOOH electrodes (coated on GCE).

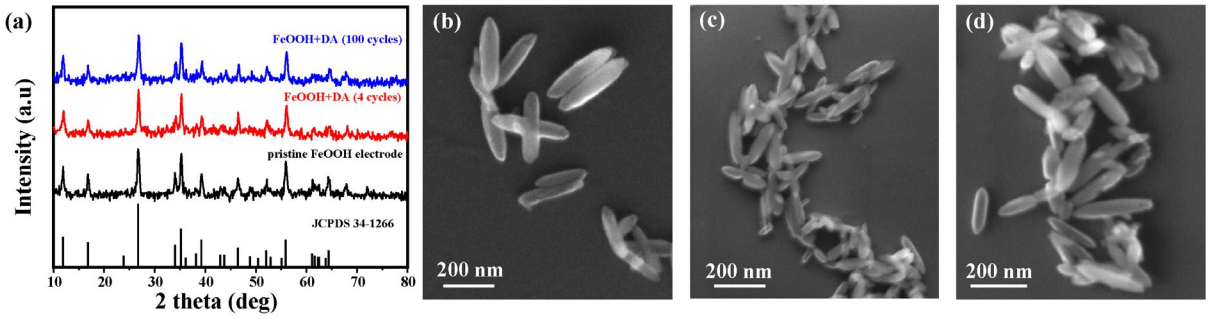

Figure S10. Stability of FeOOH electrode: (a) XRD patterns and (b, c, d) FESEM images of pristine β-FeOOH electrode, post-DA sensing (4 cycles) electrode and electrode after 100 cycles respectively.

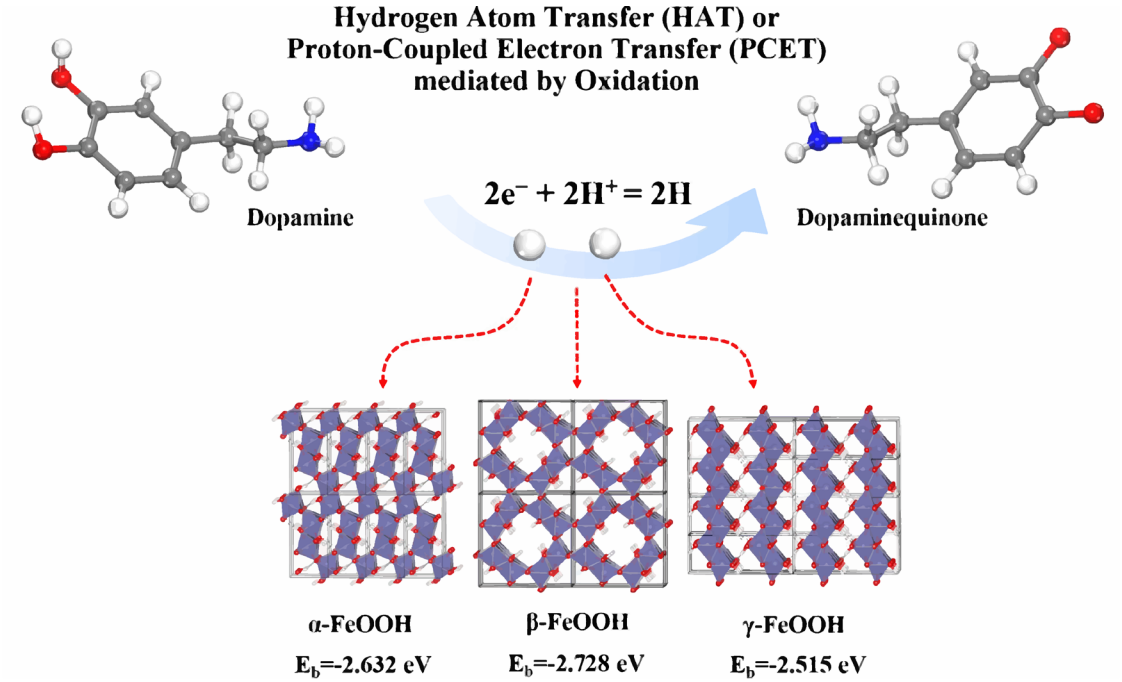

Figure S11. Oxidation mediated dopamine sensing mechanism through hydrogen atom transfer (HAT) or proton-coupled electron transfer (PCET).

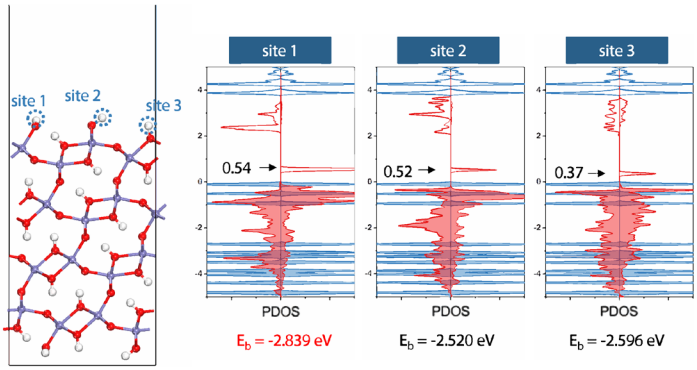

Figure S12. Surface structures (left) and partial density of states (PDOS) with hydrogen atom binding energies (E_b) on denoted oxygen sites of α-FeOOH (101) plane. Red and blue plots in PDOS represent FeOOH and dopamine respectively.

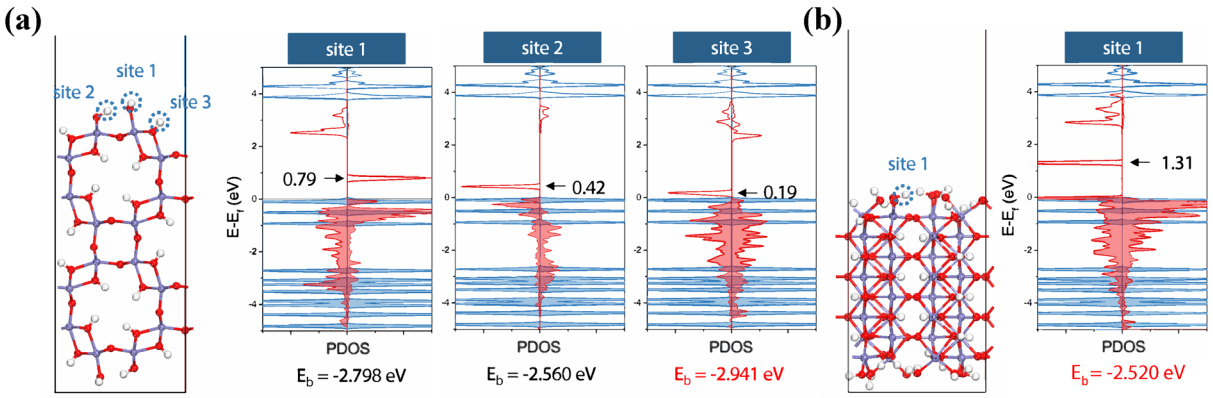

Figure S13. Surface structures (left) and partial density of states (PDOS) with hydrogen atom binding energies (E_b) on denoted oxygen sites of β-FeOOH (a) (100) and (b) (010) planes. Red and blue plots in PDOS represent FeOOH and dopamine respectively.

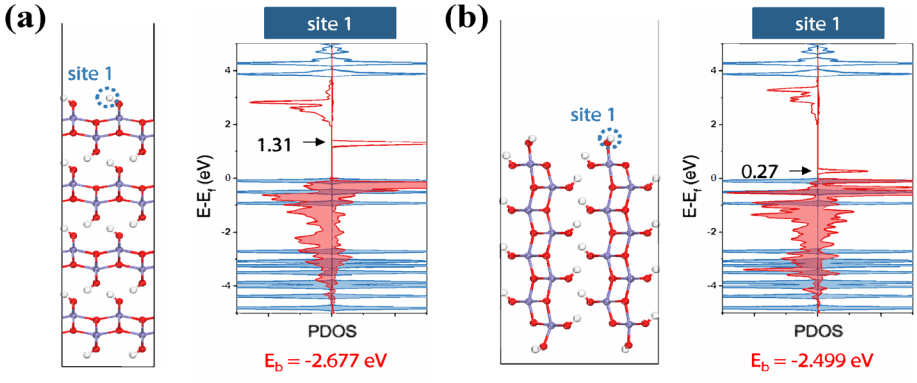

Figure S14. Surface structures (left) and partial density of states (PDOS) with hydrogen atom binding energies (E_b) on denoted oxygen sites of γ-FeOOH (a) (010) and (b) (001) planes. Red and blue plots in PDOS represent FeOOH and dopamine respectively.

Table S4. Hydrogen atom binding energies (E_b) on denoted oxygen sites of FeOOH planes.

Electrocatalyst	**Surface**	**Binding site**	**HOMO-CBM gap (eV)**	**E_b**
α-FeOOH	101	Site 1	0.54	-2.839
		Site 2	0.52	-2.520
		Site 3	0.37	-2.596
	111	Site 1	0.93	-2.899
		Site 2	0.51	-2.364
	avg.			**-2.644**
β-FeOOH	100	Site 1	0.79	-2.798
		Site 2	0.42	-2.560
		Site 3	0.19	-2.941
	010	Site 1	1.31	-2.520
	211	Site 1	0.90	-2.525
		Site 2	0.14	-2.781
		Site 3	0.19	-3.035
		Site 4	0.47	-2.801
		Site 5	1.35	-2.496
	avg.			**-2.717**
γ-FeOOH	010	Site 1	0.27	-2.499
	001	Site 1	1.31	-2.677
	031	Site 1	0.93	-2.769
		Site 2	0.61	-2.523
		Site 3	0.29	-2.254
	avg.			**-2.545**

References:

[1] Z. Rui, W. Huang, Y. Chen, K. Zhang, Y. Cao, J. Tu, Facile synthesis of graphene/polypyrrole 3 D composite for a high-sensitivity non-enzymatic dopamine detection, J. Appl. Polym. Sci. 134 (2017) 44840.

[2] D. Rao, X. Zhang, Q. Sheng, J. Zheng, Highly improved sensing of dopamine by using glassy carbon electrode modified with MnO 2, graphene oxide, carbon nanotubes and gold nanoparticles, Microchim. Acta. 183 (2016) 2597–2604.

[3] S. Zhang, Y. Fu, Q. Sheng, J. Zheng, Nickel–cobalt double hydroxide nanosheets wrapped amorphous Ni (OH) 2 nanoboxes: development of dopamine sensor with enhanced electrochemical properties, New J. Chem. 41 (2017) 13076–13084.

[4] K. Khun, Z.H. Ibupoto, X. Liu, N.A. Mansor, A.P.F. Turner, V. Beni, M. Willander, An electrochemical dopamine sensor based on the ZnO/CuO nanohybrid structures, J. Nanosci. Nanotechnol. 14 (2014) 6646–6652.

[5] G. Xu, Z.A. Jarjes, V. Desprez, P.A. Kilmartin, J. Travas-Sejdic, Sensitive, selective, disposable electrochemical dopamine sensor based on PEDOT-modified laser scribed graphene, Biosens. Bioelectron. 107 (2018) 184–191.

[6] M. Li, J.E. Zhu, L. Zhang, X. Chen, H. Zhang, F. Zhang, S. Xu, D.G. Evans, Facile synthesis of NiAl-layered double hydroxide/graphene hybrid with enhanced electrochemical properties for detection of dopamine, Nanoscale. 3 (2011) 4240–4246.

[7] G.P. Keeley, N. McEvoy, H. Nolan, S. Kumar, E. Rezvani, M. Holzinger, S. Cosnier, G.S. Duesberg, Simultaneous electrochemical determination of dopamine and paracetamol based on thin pyrolytic carbon films, Anal. Methods. 4 (2012) 2048–2053.

[8] J. Yang, J.R. Strickler, S. Gunasekaran, Indium tin oxide-coated glass modified with reduced graphene oxide sheets and gold nanoparticles as disposable working electrodes for dopamine sensing in meat samples, Nanoscale. 4 (2012) 4594–4602.

[9] E. Scavetta, R. Mazzoni, F. Mariani, R.G. Margutta, A. Bonfiglio, M. Demelas, S. Fiorilli, M. Marzocchi, B. Fraboni, Dopamine amperometric detection at a ferrocene clicked PEDOT: PSS coated electrode, J. Mater. Chem. B. 2 (2014) 2861–2867.

[10] J. Zhang, X. Bai, T. Wang, W. Xiao, P. Xi, J. Wang, D. Gao, J. Wang, Bimetallic nickel cobalt sulfide as efficient electrocatalyst for Zn–air battery and water splitting, Nanomicro Lett. 11 (2019) 2.

[11] C.G. Zoski, Handbook of electrochemistry, Elsevier, 2006.